**Original Article**

# Optimizing Image Reconstruction Parameters in Time of Flight PET/CT Imaging: a Phantom Study

**Mahnaz Shekari[1, 2], Pardis Ghafarian[3, 4, *], Sahar Ahangari[1, 2], Hossein Ghadiri[1, 2], Mehrdad Bakhshayeshkaram[3, 4], and Mohammad Reza Ay[1, 2]**

1- Department of Medical Physics and Biomedical Engineering, Tehran University of Medical Sciences, Tehran, Iran.

2- Research Center for Molecular and Cellular Imaging, Tehran University of Medical Sciences, Tehran, Iran.

3- Chronic Respiratory Diseases Research Center, National Research Institute of Tuberculosis and Lung Diseases (NRITLD), Shahid Beheshti University of Medical Sciences, Tehran, Iran.

4- PET/CT and Cyclotron Center, Masih Daneshvari Hospital, Shahid Beheshti University of Medical Sciences, Tehran, Iran.

# A B S T R A C T

**Purpose-** The aim of this study was to determine optimal reconstruction parameters in relation to the image quality and quantitative accuracy for advanced reconstruction algorithms by phantom study.

**Methods-** A house-made image quality phantom, including 6 cylindrical inserts, was filled with an $^{18}$F-FDG solution with a 4:1 radioactivity ratio compared to the background. All emission data was acquired in 3D list-mode. The PET data reconstructed with TOF only and TOF+PSF algorithms. The reconstructed images were post-filtered with Gaussian filters with varying FWHM (0 to 10 mm with 0.5 mm increment). All images were reconstructed with different product of iterations and subsets ($It \times SS$) ranging from 3 to 144. Optimal image reconstruction parameters were determined by calculating quantitative parameters including noise, signal to noise ratio (SNR), and recovery coefficient (RC).

**Results-** Our results showed that Gaussian filtering with FWHM greater than 5 mm for TOF and greater than 3.5 mm for TOF+PSF algorithms led to an acceptable clinical noise level (<10%). By considering signal to noise ratio of the 10 mm insert ($SNR_{10\ mm}$) and quantitative accuracy of tracer concentration, optimum FWHM of Gaussian filter was 5-6.5 mm for TOF only reconstruction and 3.5-5 mm for TOF+PSF reconstruction. In terms of $It \times SS$, $SNR_{10\ mm}$ was maximized for 28 to 48 $It \times SS$. In addition, there was no significant enhancement in RC for $It \times SS$ greater than 48.

**Conclusion-** Image quality and quantitative accuracy are strongly influenced by reconstruction parameters. Our findings indicate that the optimization of the reconstruction parameters is necessary to obtain the best performance. Optimal FWHM range was 5-6.5 mm for TOF only reconstruction, and 3.5-5 mm for TOF+PSF reconstruction. Additionally, due to intensifying signal of the focal point by incorporating TOF information, faster SNR convergence can be achieved. Hence smaller $It \times SS$ can be applied while using TOF algorithm for image reconstruction.

## 1. Introduction

$^{18}$F-FDG PET imaging is a clinical tool widely used in oncology, cardiology and neurology [1-4]. As an analogue of glucose, uptake of $^{18}$F-FDG provides an indication of glucose metabolism throughout the body and enables clinicians to detect regions of hyper-metabolism [5], that may indicate cancer, or regions of hypo-metabolism, that may indicate necrosis [6] or be characteristic of certain forms of dementia [7, 8]. While a qualitative assessment of oncological PET images is often sufficient for lesion detection and diagnosis [9],

*Corresponding Author:*
*Pardis Ghafarian, PhD*
*Shahid Beheshti University of Medical Sciences, Masih Daneshvari Hospital, Tehran, Iran.*
*Tel: (+98) 2166907532 /Fax: (+98) 2166581553*
*Email: pardis.ghafarian@sbmu.ac.ir*

the assessment of treatment response, especially predicting response during treatment, requires a quantitative assessment of changes in ^{18}F-FDG uptake. The most widely used (semi-) quantitative index for evaluating static PET images is the Standardized Uptake Value (SUV). SUV provides a normalized measure of radiotracer uptake that enables comparison across scans and between patients. Although, SUV is prone to intra- and inter-individual biases by a broad range of biological and technical factors [10-12]. It can be affected by patient characteristics e.g. patient weight, blood glucose level and respiratory movements as well as acquisition and reconstruction parameters like uptake time, decay correction, inaccurate calibration of the PET scanner or use of contrast agent in PET/CT imaging [10, 11]. Therefore, different scanner types and reconstruction parameters which influence sensitivity of PET, signal-to-noise ratio (SNR) and image size, have been shown to affect SUV quantification. In detail, varying numbers of iterations and subsets in the ordered subset expectation maximization (OSEM) algorithm, employing 2D or 3D reconstruction, different matrix sizes and application of smoothing filters influence SUV quantification [13-17].

Nowadays, with the advent of fast scintillators, improvements in electronics, availability of cheaper computing power, and advancements in reconstruction methods, Time-of-flight (TOF) PET and Point Spread Function modelling, are widely used as new standard reconstruction methods for all major clinical PET/CT imaging [18-22]. These new algorithms have been developed to improve signal to noise ratio and spatial resolution [23-25]. TOF PET detects time difference between the arrival times of coincident photons along a line of response and uses this information to localize the position of the positron annihilation [18]. Time-of-flight has been reported to improve image SNR and lesion detectability [23, 24]. Point-spread function modeling includes the response of point sources located throughout the scanner FOV. By using a reconstruction algorithm with PSF modeling, the lines of response can be relocated to their actual position. Therefore, PSF improves the spatial resolution and SNR of PET images [26, 27].

Recently, several approaches have been published to address the issue of reconstruction-dependent variation of SUV [28-30]. For achieving the best performance of these reconstruction algorithms, including a better image quality and more accurate quantification, it is crucial to optimize reconstruction parameters [31]. The aim of this study was to determine optimal reconstruction parameters for TOF and TOF+PSF algorithms which implemented in our PET/CT scanner using dedicated phantom study. The motivation behind this study was to optimize the number of iterations, subsets, and post-smoothing filter which may strongly influence image quality and quantification in PET images.

## 2. Materials and Methods

### 2.1. Scanner

In this study, all PET/CT scans were performed on a GE Discovery 690 PET/CT scanner. This PET scanner comprises of 24 rings with a total of 13824 LBS-Lutetium based scintillator detectors, covering an axial FOV of 15.7 cm and a trans-axial FOV of 70 cm in diameter; each block is $4.2 \times 6.2 \times 25$ mm$^3$. The coincidence time window in this scanner set to 4.9 ns and the TOF timing resolution is almost 555 ps. Each scan was acquired using the standard clinical "skull base to mid-thigh" (SBMT) protocol with all corrections (attenuation correction, random correction, scatter correction, dead-time correction, and decay correction). The PET data were acquired in 3D static list-mode. A whole-body CT scan for the attenuation correction was performed using 120 kV, 100 mA, with 3.75 mm slice thickness.

### 2.2. Phantom

In this study, an in-house image quality phantom, with a volume of 9.18 liters and 6 fillable cylindrical inserts, was used (Figure 1). Internal diameter of inserts were 10, 13, 17, 22, 28, and 37 mm. A cylindrical insert ($5.0 \pm 0.2$ cm outside diameter) filled with a low atomic number material that mimics lung attenuation (average density of $0.3 \pm 0.1$ g/mL) is centered inside the 'body compartment', and extends axially through the entire phantom. In order to achieve liver uptake of a 70 kg patient, its compartment was filled with 5.3 kBq/ml ^{18}F-FDG solution [32]. Cylindrical inserts were filled with ^{18}F-FDG solution with 4:1 activity ratio with respect to the background.
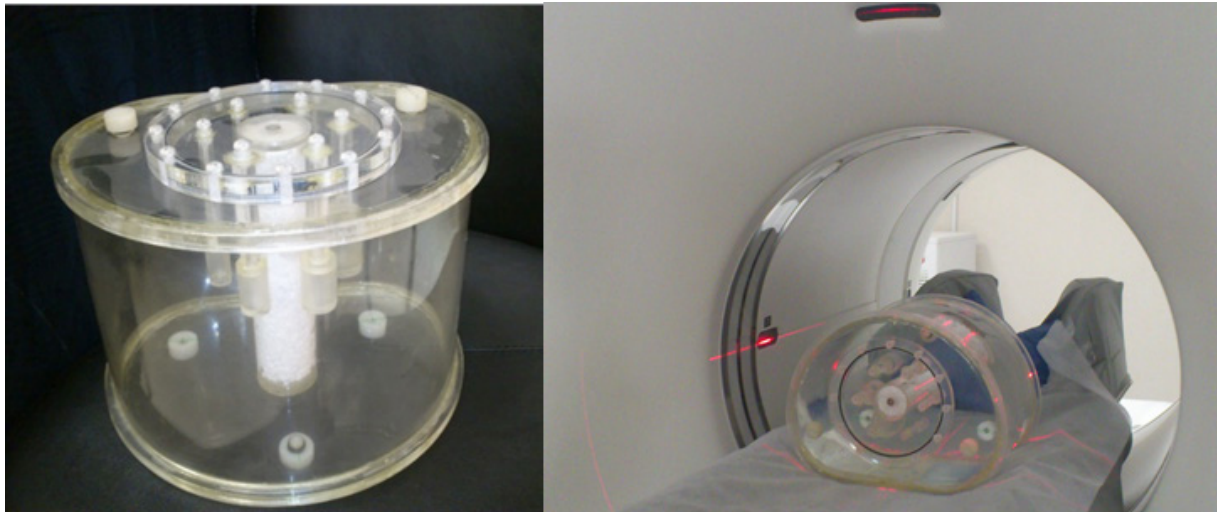
**Figure 1.** Image Quality phantom (Left). Preparing image quality phantom to initiate PET scan (Right).

## 2.3. Reconstruction Parameters

Emission scan acquired in 3D list mode for 180 s. Using list mode data acquisition, additional information such as the time and energy of each detected photon can also be stored. The list-mode output data were used for image reconstruction. All PET data were reconstructed with TOF algorithm and PSF-modelling reconstruction. In the first step, all images reconstructed with 2 Iterations and 24 subsets. In order to assess the impact of filter size, Post-smoothing filters with FWHM ranging from 0 to 10 mm with 0.5 mm increment applied to all images. In the second study, the impact of the number of iterations and subsets on image quality parameters were assessed. We will refer to subsets and iterations as *It×SS*, as the product of OSEM subsets and iterations is comparable to the total number of MLEM iterations for lower numbers of iterations [33]. All images reconstructed with *It×SS* ranging from 3 to 144. Matrix-size of all images were 256×256.

## 2.4. Data Analysis

Image quality was assessed by SNR of 10 mm hot insert and noise in the background. Noise was calculated by drawing 12 circular ROIs with 37 mm in diameter placed in central slice and ±2 slices away of it. Total 60 ROIs were drawn and noise was defined as below:

$$\text{Noise} = \frac{SD(Background)}{C(Background)} \times 100 \qquad (1)$$

Where $C_{Background}$ is the average activity and

$SD_{Background}$ is the average of resultant SD within 60 circular ROIs.

The signal to noise ratio of a 10 mm diameter hot insert ($SNR_{10\,mm}$), as an image quality metric, was calculated as follow:

$$SNR(10mm) = \frac{C(max) - C(Background)}{SD(Background)} \qquad (2)$$

Where C (max) is the maximum activity concentration at drawn VOI which comprehensively covers insert's volume.

To evaluate the accuracy of measured activity concentration in hot inserts of reconstructed images, the recovery coefficient of smallest insert (RC) computed as below:

$$RC = \frac{C(Isocontour50\%)}{T} \times 100 \qquad (3)$$

Where C is the average activity concentration within voxels which have the values higher than 50% maximum voxel value, in a drawn VOI [13]. T represents the true activity concentration.

## 3. Results

The noise variation in phantom images in relation to FWHM of post-smoothing filter was plotted in Figure 2. It was shown that by increasing FWHM of Gaussian filter, noise decreased, which can be interpreted as a more uniform background. Figure 3 shows $SNR_{10\,mm}$ against noise for images reconstructed with different filter size. It was demonstrated that by increasing the filter size,

$SNR_{10\,mm}$ reached the maximum point, then by increasing the filter size, fell off. A compromise trade-off between the noise level and $SNR_{10\,mm}$ revealed that the optimized filter size was ranging from 5 to 6.5 mm and 3.5 to 5 mm for TOF and TOF+PSF algorithms respectively. Recovery coefficients for all 6 inserts are reported for post-smoothing filters with 2, 4, and 6 mm FWHM in

Table 1. For the smallest insert, RC decreased up to 32% by increasing FWHM of Gaussian from 2 mm to 6 mm. The PET images reconstructed using various FWHMs of the Gaussian filter are shown in Figure 4 where by increasing FWHM of Gaussian filter, the background uniformity improves in expense of blurring insert's edge especially for the smallest insert (10 mm).
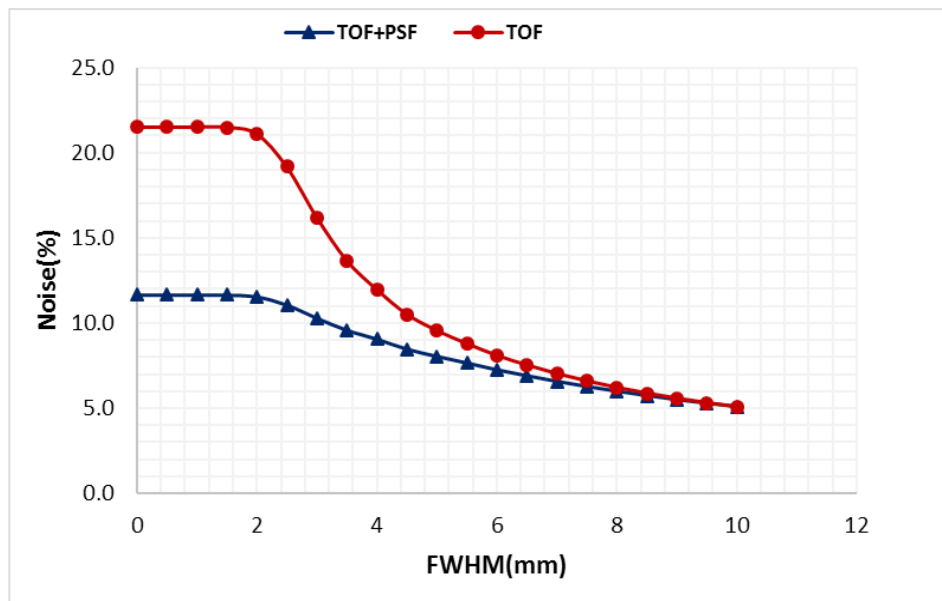


**Figure 2.** Noise trends against different filter size for PET images reconstructed with TOF and TOF+PSF algorithms.
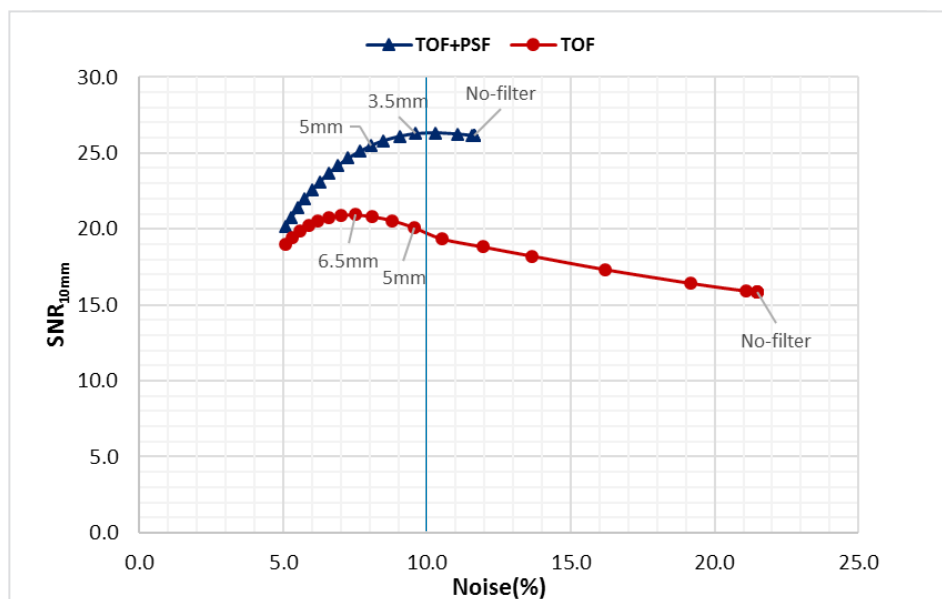


**Figure 3.** $SNR_{10\,mm}$ against noise for PET images reconstructed with TOF and TOF+PSF algorithms. Each point shows a filter size ranging from 0 to 10 mm with 0.5 mm increment.

Table 1. RC% of all inserts resulted from 2, 4, and 6 mm FWHM of post-smoothing filter.

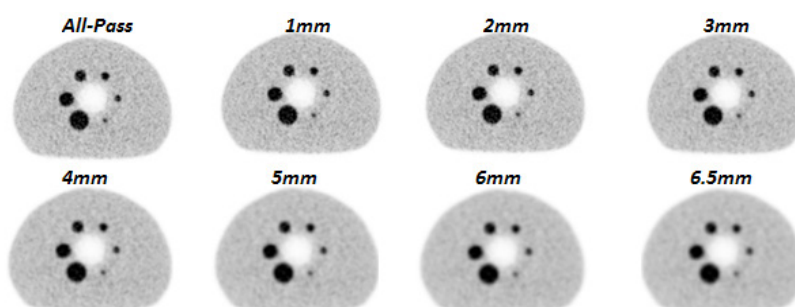| FWHM (mm) | 2 | | 4 | | 6 | |
|---|---|---|---|---|---|---|
| Insert Diameter (mm) | TOF | TOF+PSF | TOF | TOF+PSF | TOF | TOF+PSF |
| 10 | 76.3 | 73.9 | 58.7 | 60.1 | 49.9 | 51.2 |
| 13 | 80.4 | 83.6 | 68.9 | 73.8 | 60.2 | 64.6 |
| 17 | 85.2 | 88.2 | 75.5 | 80.3 | 68.5 | 73.2 |
| 22 | 87.7 | 89.2 | 79.8 | 83.2 | 74.2 | 78.3 |
| 28 | 89.5 | 88.7 | 82.3 | 85.3 | 78.7 | 82 |
| 37 | 92.5 | 92.7 | 86.2 | 89 | 82.4 | 85.7 |



**Figure 4.** Transverse PET images of image quality phantom for 4:1 contrast, reconstructed with TOF algorithm, and different size of post-smoothing filters.

The PET images reconstructed with TOF algorithm by various $It \times SS$ are shown in Figure 5. It can be seen that by increasing $It \times SS$, the image convergence improves, but subsequently the noise increases. To determine optimal $It \times SS$, $SNR_{10\ mm}$ versus noise were plotted. Figure 6 showed for $It \times SS$ ranged from 28 to 48, $SNR_{10\ mm}$ is at highest values for both TOF and TOF+PSF algorithms. For $It \times SS$ greater than 48, due to more noise propagation, $SNR_{10\ mm}$ dropped-off. Figure 7 showed RC is affected by the number of iterations and subsets. For TOF algorithm, by achieving 64 ($It \times SS$), the curve became plateau, but for TOF+PSF, due to additional information of PSF algorithm, RC enhancement was continued up to 144 ($It \times SS$).

Figure 8 shows clinical PET images reconstructed with optimal reconstruction parameters for TOF algorithm (including $It \times SS$ ranging from 24 to 48, and a Gaussian filter with a FWHM of 5 mm). It shows that by increasing $It \times SS$, there was no gain in lesion over background ratio (LBR). On the other hand, noise enhances by increasing $It \times SS$. However, for clinical PET images, optimal range for $It \times SS$ is probably smaller (It×SS ranging from 24-36).
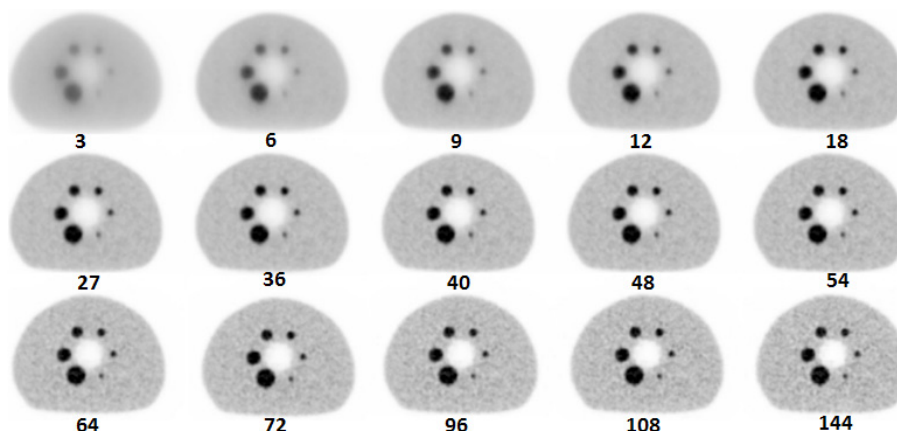


**Figure 5.** Transverse PET images of phantom reconstructed with TOF algorithm for different $It \times SS$ (4:1 contrast).
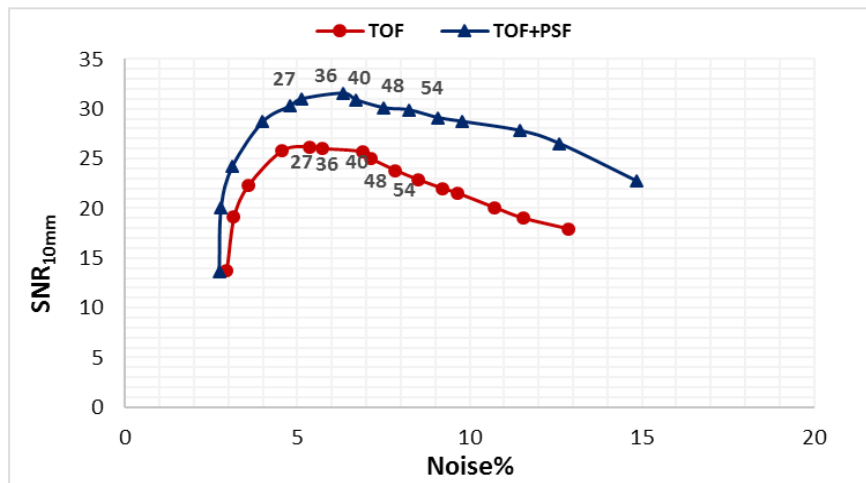
**Figure 6.** $SNR_{10\ mm}$ versus image noise% for phantom images reconstructed with TOF and TOF+PSF algorithms for different Iteration×Subset.
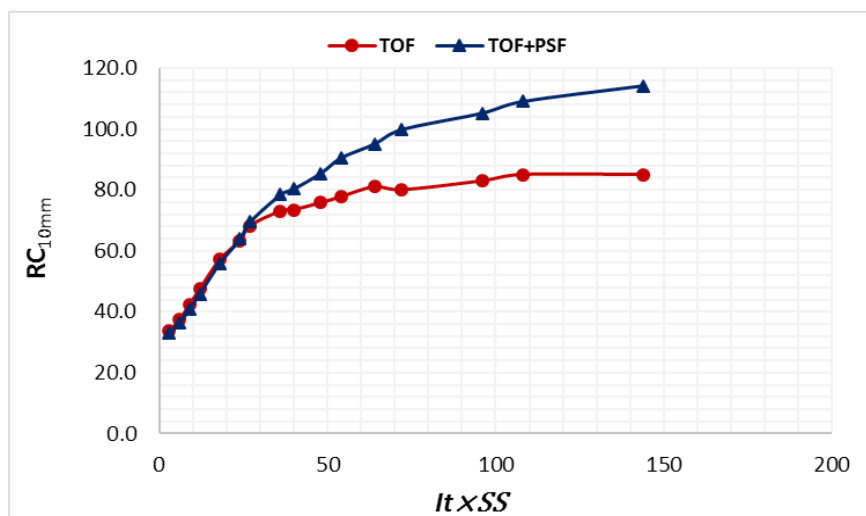


**Figure 7.** $RC_{10\ mm}$ versus $It \times SS$ for phantom images reconstructed with TOF, and TOF+PSF algorithms.
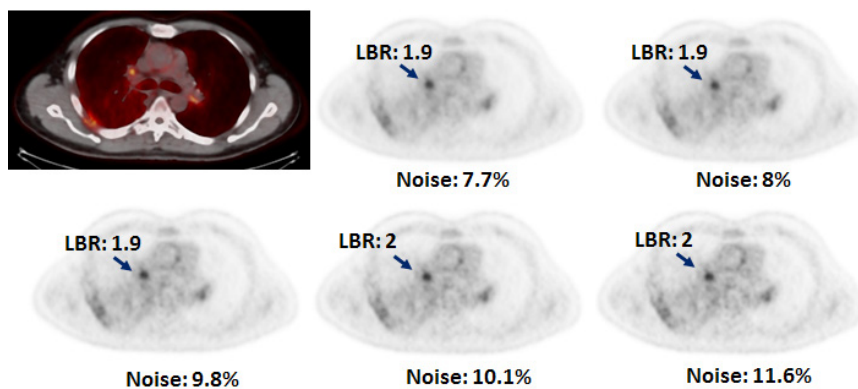


**Figure 8.** Patient images reconstructed with TOF algorithm (Injected dose= 377.4 MBq, BMI= 28.1). First row: Fused PET/CT, images reconstructed with 24 and 27 $It \times SS$. Second row: images reconstructed with 36, 40, and 48 $It \times SS$. A post smoothing filter with a FWHM of 5 mm was applied to all images.

## 4. Discussion

In this study, we evaluated the impact of reconstruction parameters on the image quality and quantification for TOF and TOF+PSF algorithms using phantom study. As the image pixel size was 2.74 mm, the noise for both algorithms were constant up to 2.5 mm FWHM of post-smoothing filter. Then, as the FWHM of the Gaussian filter increases, the smoothing strength of the filter is also increased (more noise is removed) but it will also lead to increased image blurring. When the width of the Gaussian fit curve decreases, the filter is able to compute fewer voxels/regions in the image which is capable of producing less error than computing larger voxel regions. In that regard, small tumor in clinical imaging may benefit if a filter with smaller FWHM is used instead of using filters with larger FWHMs, especially when there is a poor image contrast. The noise of all TOF images were higher in compare with TOF+PSF algorithm [25, 34]. Therefore, the size of FWHM of Gaussian filter has more effect on the image quality and quantification for TOF images. By increasing FWHM of Gaussian filters and subsequently suppressing noise of PET images, firstly $SNR_{10\,mm}$ improves and reaches maximum value, and then, by increasing the filter size, in addition to noise suppression, voxel counts was underestimated, which leads to SNR degradation (Figure 3). In our study, it was shown that by increasing the size of FWHM of Gaussian filter, RC as a result of smoothing image, decreased. RC decreasing was more severe in smallest hot insert (32% by increasing filter size of 2 mm to 6 mm). Therefore, it can be concluded that by increasing the filter size, the activity concentration of small lesion will be underestimated.

Our results showed increasing $It{\times}SS$, generally enhances the noise [33], but SNR trend was completely different. By increasing $It{\times}SS$, the signal will be intensified, and subsequently SNR increased till reaching the maximum value. After maximum point, due to noise enhancement, SNR degraded. So for achieving good image quality, it is mandatory to choose reconstruction parameters with the best SNR and acceptable noise level (<10%). Calculated RC against $It{\times}SS$ for images reconstructed with TOF algorithm revealed that RC did not change significantly after 54 $It{\times}SS$.

Hence, reconstructing images with $It{\times}SS$ greater than 54, there would be no gain in the accuracy of RC, which is due to faster convergence of TOF images, as shown in previous study [25, 35]. Furthermore, TOF+PSF converge slowly due to additional information of object to be recovered [34].

Image quality and quantitative accuracy are strongly influenced by reconstruction parameters. Our findings indicate that the optimization of reconstruction parameters is necessary to obtain the best performance. Optimum filter size was 5-6.5 mm for TOF reconstruction, and 3.5-5 mm for TOF+PSF reconstruction. Additionally, due to the intensifying signal of focal point by incorporating TOF information, faster image convergence can be achieved. Hence, smaller $It{\times}SS$ can be applied while using TOF algorithm for image reconstruction.

## Acknowledgment

## References

1- D. Delbeke, "Oncological applications of FDG PET imaging: brain tumors, colorectal cancer lymphoma and melanoma," *The Journal of Nuclear Medicine,* vol. 40, p. 591, 1999.

2- R. J. Hicks, V. Kalff, M. P. MacManus, R. E. Ware, A. F. McKenzie, J. P. Matthews, *et al.*, "The utility of 18F-FDG PET for suspected recurrent non–small cell lung cancer after potentially curative therapy: impact on management and prognostic stratification," *Journal of Nuclear Medicine,* vol. 42, pp. 1605-1613, 2001.

3- W. J. Oyen, J. Bussink, A. F. Verhagen, F. H. Corstens, and G. P. Bootsma, "Role of FDG-PET in the diagnosis and management of lung cancer," 2004.

4- J. Vansteenkiste, B. M. Fischer, C. Dooms, and

J. Mortensen, "Positron-emission tomography in prognostic and therapeutic assessment of lung cancer: systematic review," *The lancet oncology,* vol. 5, pp. 531-540, 2004.

5- F. Vollenweider, K. Leenders, C. Scharfetter, A. Antonini, P. Maguire, J. Missimer*, et al.*, "Metabolic hyperfrontality and psychopathology in the ketamine model of psychosis using positron emission tomography (PET) and [18 F] fluorodeoxyglucose (FDG)," *European Neuropsychopharmacology,* vol. 7, pp. 9-24, 1997.

6- D. Delbeke, R. E. Coleman, M. J. Guiberteau, M. L. Brown, H. D. Royal, B. A. Siegel*, et al.*, "Procedure guideline for tumor imaging with 18F-FDG PET/CT 1.0," *Journal of Nuclear Medicine,* vol. 47, pp. 885-895, 2006.

7- J. M. Hoffman, K. A. Welsh-Bohmer, M. Hanson, B. Crain, C. Hulette, N. Earl*, et al.*, "FDG PET imaging in patients with pathologically verified dementia," *Journal of Nuclear Medicine,* vol. 41, pp. 1920-1928, 2000.

8- D. H. Silverman, "Brain 18F-FDG PET in the diagnosis of neurodegenerative dementias: comparison with perfusion SPECT and with clinical evaluations lacking nuclear imaging," *Journal of Nuclear Medicine,* vol. 45, pp. 594-607, 2004.

9- H. Jadvar and J. A. Parker, *Clinical PET and PET/CT*: Springer Science & Business Media, 2006.

10- R. Boellaard, "Standards for PET image acquisition and quantitative data analysis," *Journal of nuclear medicine,* vol. 50, pp. 11S-20S, 2009.

11- M. C. Adams, T. G. Turkington, J. M. Wilson, and T. Z. Wong, "A systematic review of the factors affecting accuracy of SUV measurements," *American Journal of Roentgenology,* vol. 195, pp. 310-320, 2010.

12- D. Vriens, E. P. Visser, L.-F. de Geus-Oei, and W. J. Oyen, "Methodological considerations in quantification of oncological FDG PET studies," *European journal of nuclear medicine and molecular imaging,* vol. 37, pp. 1408-1425, 2010.

13- R. Boellaard, N. C. Krak, O. S. Hoekstra, and A. A. Lammertsma, "Effects of noise, image resolution, and ROI definition on the accuracy of standard uptake values: a simulation study," *Journal of Nuclear Medicine,* vol. 45, pp. 1519-1527, 2004.

14- C. J. Jaskowiak, J. A. Bianco, S. B. Perlman, and J. P. Fine, "Influence of reconstruction iterations on 18F-FDG PET/CT standardized uptake values," *Journal of Nuclear Medicine,* vol. 46, pp. 424-428, 2005.

15- M. A. Lodge, M. A. Chaudhry, and R. L. Wahl, "Noise considerations for PET quantification using maximum and peak standardized uptake value," *Journal of Nuclear Medicine,* vol. 53, pp. 1041-1047, 2012.

16- G. Akamatsu, K. Mitsumoto, T. Taniguchi, Y. Tsutsui, S. Baba, and M. Sasaki, "Influences of point-spread function and time-of-flight reconstructions on standardized uptake value of lymph node metastases in FDG-PET," *European journal of radiology,* vol. 83, pp. 226-230, 2014.

17- E. Prieto, I. Domínguez-Prado, M. J. García-Velloso, I. Peñuelas, J. Á. Richter, and J. M. Martí-Climent, "Impact of time-of-flight and point-spread-function in SUV quantification for oncological PET," *Clinical nuclear medicine,* vol. 38, pp. 103-109, 2013.

18- T. K. Lewellen, "Time-of-flight PET," in *Seminars in nuclear medicine*, 1998, pp. 268-275.

19- M. Conti, "State of the art and challenges of time-of-flight PET," *Physica Medica,* vol. 25, pp. 1-11, 2009.

20- B. Jakoby, Y. Bercier, M. Conti, M. Casey, B. Bendriem, and D. Townsend, "Physical and clinical performance of the mCT time-of-flight PET/CT scanner," *Physics in medicine and biology,* vol. 56, p. 2375, 2011.

21- S. Surti, A. Kuhn, M. E. Werner, A. E. Perkins, J. Kolthammer, and J. S. Karp, "Performance of Philips Gemini TF PET/CT scanner with special consideration for its time-of-flight imaging capabilities," *Journal of Nuclear Medicine,* vol. 48, pp. 471-480, 2007.

22- V. Bettinardi, L. Presotto, E. Rapisarda, M. Picchio, L. Gianolli, and M. Gilardi, "Physical performance of the new hybrid PET/CT Discovery-690," *Medical physics,* vol. 38, pp. 5394-5411, 2011.

23- V. Y. Panin, F. Kehren, C. Michel, and M. Casey, "Fully 3-D PET reconstruction with system matrix derived from point source measurements," *Medical Imaging, IEEE Transactions on,* vol. 25, pp. 907-921, 2006.

24- A. M. Alessio, C. W. Stearns, S. Tong, S. G. Ross, S. Kohlmyer, A. Ganin*, et al.*, "Application and evaluation of a measured spatially variant system model for PET image reconstruction," *Medical Imaging, IEEE Transactions on,* vol. 29, pp. 938-949, 2010.

25- C. Lois, B. W. Jakoby, M. J. Long, K. F. Hubner, D. W. Barker, M. E. Casey, *et al.*, "An assessment of the impact of incorporating time-of-flight information into clinical PET/CT imaging," *Journal of Nuclear Medicine,* vol. 51, pp. 237-245, 2010.

26- S. Tong, A. Alessio, and P. Kinahan, "Noise and signal properties in PSF-based fully 3D PET image reconstruction: an experimental evaluation," *Physics in medicine and biology,* vol. 55, p. 1453, 2010.

27- A. Varrone, N. Sjöholm, L. Eriksson, B. Gulyás, C. Halldin, and L. Farde, "Advancement in PET quantification using 3D-OP-OSEM point spread function reconstruction with the HRRT," *European journal of nuclear medicine and molecular imaging,* vol. 36, pp. 1639-1650, 2009.

28- A. Joshi, R. A. Koeppe, and J. A. Fessler, "Reducing between scanner differences in multi-center PET studies," *Neuroimage,* vol. 46, pp. 154-159, 2009.

29- M. D. Kelly and J. M. Declerck, "SUVref: reducing reconstruction-dependent variation in PET SUV," *EJNMMI research,* vol. 1, pp. 1-11, 2011.

30- R. Boellaard, M. J. O'Doherty, W. A. Weber, F. M. Mottaghy, M. N. Lonsdale, S. G. Stroobants, *et al.*, "FDG PET and PET/CT: EANM procedure guidelines for tumour PET imaging: version 1.0," *European journal of nuclear medicine and molecular imaging,* vol. 37, pp. 181-200, 2010.

31- G. Akamatsu, K. Ishikawa, K. Mitsumoto, T. Taniguchi, N. Ohya, S. Baba, *et al.*, "Improvement in PET/CT image quality with a combination of point-spread function and time-of-flight in relation to reconstruction parameters," *Journal of Nuclear Medicine,* vol. 53, pp. 1716-1722, 2012.

32- N. Paquet, A. Albert, J. Foidart, and R. Hustinx, "Within-patient variability of 18F-FDG: standardized uptake values in normal tissues," *Journal of Nuclear Medicine,* vol. 45, pp. 784-788, 2004.

33- H. M. Hudson and R. S. Larkin, "Accelerated image reconstruction using ordered subsets of projection data," *Medical Imaging, IEEE Transactions on,* vol. 13, pp. 601-609, 1994.

34- K. Thielemans, E. Asma, S. Ahn, R. Manjeshwar, T. Deller, S. Ross, *et al.*, "Impact of PSF modelling on the convergence rate and edge behaviour of EM images in PET," in *Nuclear Science Symposium Conference Record (NSS/MIC), 2010 IEEE*, 2010, pp. 3267-3272.

35- J. S. Karp, S. Surti, M. E. Daube-Witherspoon, and G. Muehllehner, "Benefit of time-of-flight in PET: experimental and clinical results," *Journal of Nuclear Medicine,* vol. 49, pp. 462-470, 2008.